Neutron angular and energy distributions from 710-MeV alphas stopping in water, carbon, steel, and lead, and 640-MeV alphas stopping in lead

R. A. Cecil, B. D. Anderson, A. R. Baldwin, and R. Madey
Department of Physics, Kent State University, Kent, Ohio 44242

A. Galonsky, P. Miller, and L. Young*
Cyclotron Laboratory, Michigan State University, East Lansing, Michigan 48824

F. M. Waterman†
Department of Radiology, University of Chicago, Chicago, Illinois 60637

(Received 22 October 1979)

We measured neutron angular and energy distributions from 710-MeV alphas stopping in targets of water, carbon, steel, and lead for neutron energies from 3 MeV to above 300 MeV. We also measured neutron spectra from 640-MeV alphas stopping in lead. These spectra are similar to the 710-MeV spectra but are reduced in magnitude by about 20 percent. The angular distributions are forward peaked and have a broad bump at about 120 MeV in the 0- and 6-degree spectra. The 710-MeV integrated yields above 10 MeV are about 0.5 neutron per incident alpha, independent of the target. The measured spectra from the water target are consistent with the calculations of an intranuclear cascade model at the forward angles, but are larger than the calculations at the backward angles.

[NUCLEAR REACTIONS H_2O, C, steel, Pb(α,xn), E=710 MeV; Pb(α,xn), E = 640 MeV. Measured unidirectional spectra and yields from thick targets. Deduced total integrated neutron yields above 10 MeV. Compared spectra with intranuclear-cascade model.]

I. INTRODUCTION

We measured unidirectional neutron spectra above 3 MeV at angles ranging from 0 to 150 deg produced by 710-MeV alpha particles stopping in targets of carbon, water, steel, and lead; in addition, we report some measurements of neutron spectra produced by 640-MeV alphas stopping in lead. These measurements were made at the Space Radiation Effects Laboratory in Newport News, Virginia. They were motivated by the need for data to design shielding for the superconducting heavy-ion accelerator at Michigan State University. These data for the light targets are of interest also for estimating neutron doses produced by nuclear interactions during irradiation of cancerous tumors with alpha beams. The measured spectra from the water target are compared with those calculated from an intranuclear-cascade model.[1]

II. EXPERIMENTAL PROCEDURE

The energy of a neutron produced in the target was measured by the time-of-flight (TOF) technique. We measured the time difference between the detection of an alpha particle in a beam telescope and the detection of a neutron in one of several counters located one to five m away from the target. The neutron energy was then calculated from the TOF of the neutron measured relative to the observed prompt gamma peak. Absolute neutron yields were determined from the number of incident alphas counted in the beam telescope and from the detection efficiency for each neutron counter as calculated with the computer code of Cecil *et al.*[2]

A. Experimental arrangement

Figure 1 shows the experimental arrangement and indicates a typical placement of five neutron counters. As many as six counters were used simultaneously during the experimental run. A 710-MeV alpha beam was extracted from the cyclotron and transported to the experimental area in an evacuated beam line. During one experimental run a copper degrader was used to reduce the 710-MeV beam to 640 MeV. The external alpha beam passed through a beam telescope consisting of two 7.6 cm by 7.6 cm by 0.79 mm thick NE-102 plastic scintillators shown as $S1$ and $S2$ in Fig. 1. Signals from $S1$ and $S2$ were used in a coincidence circuit to count the absolute number of beam particles incident on the target. The duration of the data-taking runs varied from about 1 to 4 h with a typical flux of 5×10^4 alphas per second incident on the target. After traversing

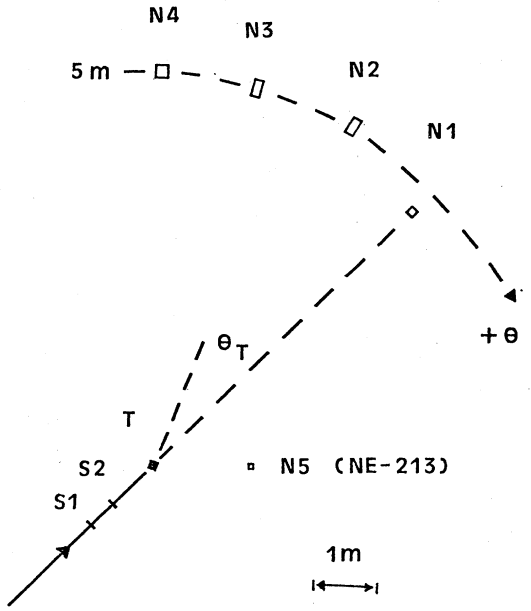

FIG. 1. The forward-angle experimental arrangement. The reference system for the target and detector angles discussed in the text is indicated.

the beam telescope, an alpha particle stopped in the target T. From geometric cross sections, we estimate that the alpha beam incident on the target had less than 1 percent contamination caused by nuclear reactions of the beam in the beam-telescope scintillators and exit window of the evacuated beam transport system. The beam spot size incident on the target was about 2 cm high by 3 cm wide. Neutrons produced in the target were detected by hydrocarbon scintillation counters. The detectors were arranged to equalize the counting rates and to provide better energy resolutions in the forward directions where there are larger yields of high-energy neutrons. The neutron flight paths were measured from the center of the target to the center of each neutron counter. The neutron counters and the target were supported by aluminum stands. The beam height was 1.5 m above the concrete floor of the experimental area. The detector angles are referenced to a spherical coordinate system with its origin at the center of the target and the positive z axis along the direction of the beam. All of the counters were in the x-z plane parallel to the floor except for the 6-deg counter which was positioned 6 deg above the beam. The NE-102 counters were deployed in two arrangements as indicated in Table I. A 5.1-cm diam by 5.1-cm thick NE-213 counter was placed at a flight path of 1 m from the target to measure the low-energy portion of the neutron spectrum; it was positioned at +45 deg in the first experimental arrangement and at either

TABLE I. NE-102 scintillator dimensions and locations.

Angle θ (deg)	Scintillator Thickness (cm)	Diameter (cm)	Flight path (m)
Arrangement 1			
0	10.2	12.7	4.9
0 (6 up)	10.2	12.7	4.9
−15	21.6	12.7	5.0
−30	21.6	12.7	5.0
−45	20.3	23.9	5.0
Arrangement 2			
−60	10.2	12.7	3.0
−90	21.6	12.7	3.0
+120	21.6	12.7	2.0
+150	20.3	20.3	2.0

0, −90, or +135 degrees in the second experimental arrangement. The NE-213 liquid scintillator was directly coupled to a 5.1-cm diam Amprex 56DVP photomultiplier tube (PMT); each of the 12.7-cm diam NE-102 scintillators was mounted directly on a 12.7-cm diam Amperex XP2041 PMT. Madey *et al.*[3] described the 22.9-cm diam NE-102 scintillator which was fitted with a tapered Plexiglass light pipe and mounted on a 12.7-cm diam 58AVP PMT. A 6.3-mm thick NE-102 plastic scintillation counter was placed immediately in front of each neutron counter to veto charged particles. In order to minimize neutron in-scattering, no local shielding was used near the counters.

B. Target dimensions and orientations

The target thicknesses and orientations are presented in Table II. The target orientation is described by the angle θ_T of the spherical coordinate system in Fig. 1. The carbon, steel, and lead targets were rectangular blocks: 15.2, 15.4, and 10.2 cm wide by 12.7, 10.2, and 10.2 cm, respectively. The water target was contained in a 22.9 cm long by 15.2-cm diam aluminum cylinder with a wall thickness of 1.4 mm. The beam entrance end of the cylinder was a 0.05 mm aluminum foil,

TABLE II. Target thicknesses and orientations.

	Carbon	Water	Steel	Lead
Thickness (g/cm^2)	25.13	22.86	34.43	44.65
(cm)	14.73	22.86	4.445	3.937
Orientation θ_T (deg)	23.5	0.0	23.5	22.5

and the exit end was a 3.2-mm thick aluminum plate.

C. Data acquisition electronics

The data acquisition system included a PDP 11/15 computer, 12 bit analog-to-digital converters, commerically available electronics, and specialized electronics developed at Kent State University to provide increased count rate and dynamic range capabilities for neutron spectral measurements. As many as six neutron counters were operated simultaneously. The anode signal from each neutron counter was split into two signals with a linear fan-out module. One signal went to a constant-fraction timing discriminator (CFD) and the other, to a wide dynamic-range stretcher module.[4] This stretcher enabled reliable pulse-height measurements over a 50:1 dynamic range. All TOF information was obtained from a single time-to-amplitude converter (TAC). The TAC was started by a signal from the output of an OR module which received the timing signal from each CFD. A fast timing signal from the beam telescope stopped the TAC. The output of the stretcher module and the TAC were processed by separate analog-to-digital converters. Pulse-height and TOF information for each counter were recorded event by event on magnetic tape by the computer; in addition, TOF and pulse-height histograms were accumulated in the computer memory and displayed on-line to monitor the operation of the detectors and to provide preliminary results.

III. DATA ANALYSIS

The event-by-event list of pulse-height and TOF data recorded on magnetic tape was analyzed off-line at Kent State University. Since pulse-height information was recorded for each TOF event, the data could be reanalyzed at any desired threshold above the hardware threshold set by the CFD for each counter. After choosing thresholds, TOF spectra were produced and backgrounds were subtracted as described below. The resulting TOF spectra were converted to energy spectra to obtain the yields reported here.

A. Background subtraction

Figure 2 is the TOF spectrum from a carbon target with the NE-102 counter at 15 deg. The estimated background, as represented by the dashed line, decreases from about 25% of the total spectrum at 14 MeV (about twice threshold), to 12% at 34 MeV, to about 2% from 68 MeV up to about 300 MeV, which energy represents the practical

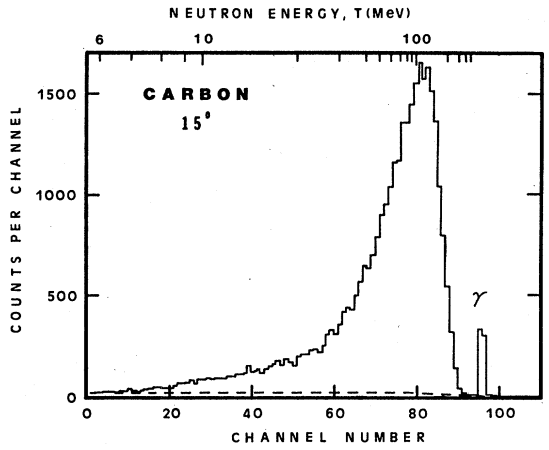

FIG. 2. The neutron time-of-flight (TOF) spectrum at 15° from 710-MeV alphas stopping in a carbon target. The dashed line represents the background that was subtracted to obtain the neutron yields. The background is a flat extrapolation from the observed background at the left of the TOF spectrum to a point at 1.2 × the most probable flight time and then sloped to the level of the background under the gamma peak. See text for discussion.

limit of our measurement of neutron yield at this angle. The spectrum shown in Fig. 2 is typical of the spectra obtained in this experiment. Because the backgrounds are relatively small, we estimated them in the following manner: In each TOF spectrum, the level of the background in the region below the discrimination threshold on the slow side of the neutron TOF spectrum was slightly higher than that on the fast side of the spectrum earlier than the gamma peak. We attributed the excess events on the slow side of the spectrum to target-induced background from room-scattered neutrons. Note that room-scattered neutron backgrounds measured by other workers[5] with shadow bars revealed similar (but larger) differences in the background levels on each side of the neutron TOF spectra. Also the magnitude of the background levels was much larger. A neutron produced in the target and scattered from the floor would have a flight time at least 1.2 times longer than a direct-path neutron of the same energy. Since such floor-scattered neutrons would dominate the room-scattered background, we estimated the background by extrapolating the flat region on the slow side of the spectrum up to a point at 1.2 times the flight time of the high-energy peak observed in the spectrum; then we extrapolated linearly down to the level observed on the fast side of the spectrum at the center of the prompt gamma-ray peak. We estimate that the (~25%) uncertainty in the background introduces an uncertainty in the extracted yields of typically less than 7%. The region of greatest

uncertainty in the background is near the assumed discontinuity where the background is always the smallest fraction (~2%) of the total spectrum.

The low-energy portions of the spectra were measured at a few angles with an NE-213 type scintillator. Although the time resolution and pulse-shape information for this detector were observed to be too poor to permit the use of n-γ discrimination for neutron spectral analysis, the pulse-shape information was used to study the γ-ray TOF spectrum. The γ-ray spectra were observed to be flat over the range from threshold to flight times corresponding to neutron energies greater than 50 MeV. Since the NE-213 detector was used to measure the spectrum only below 40 MeV, the γ-ray background was assumed to be flat and the background subtraction method described above for the NE-102 detectors was adopted also for the NE-213 data analysis. Note that γ rays from the target seen in the spectra at neutron energies above 50 MeV for the NE-213 counter at a flight path of 1 m will appear at a neutron energy above 200 MeV for an NE-102 counter at 3 m and above 500 MeV for an NE-102 counter at 5 m. Since the NE-102 counters were placed at flight paths of 3 m only for the backward angles where the neutron yield is negligible above 200 MeV, the γ-ray backgrounds for the NE-102 detectors would be expected to be flat also; moreover, the higher pulse-height thresholds adopted for the NE-102 counters (see Sec. III B below) would greatly reduce γ-ray backgrounds for these detectors.

B. Pulse-height thresholds

Before and after the experimental run, each counter was pulse-height calibrated with a series of radioactive gamma sources (viz., ^{137}Cs, ^{60}Co, ^{22}Na, and ^{228}Th); in addition, at least once every 12 h during the experimental run, each of the counters was calibrated with a ^{60}Co gamma source. The Compton peak in the gamma-ray spectrum was used as the calibration point and was associated with an equivalent-electron energy (ee) of 0.95 of the maximum Compton energy.[6] To calibrate the stretcher module and the analog-to-digital converter for large pulse heights, we used precision attenuators and a fast linear amplifier with a measured gain of 10.0 to amplify the anode signals produced in each of the neutron counters by a ^{228}Th gamma source (E_γ = 2.62 MeV). Since pulse-height information was recorded for each TOF event, the data were analyzed and compared at various pulse-height thresholds.

Yield spectra for the NE-102 counters were compared at several pulse-height thresholds ranging from 1.5 to 6.0 MeV ee. At a threshold of 1.5 MeV ee, spikes of room-scattered gammas were observed in the yield spectra. At a threshold of 3.0 MeV ee, the spikes were no longer present and the yields were consistent with the yields obtained at a 6.0-MeV ee threshold. Yield spectra were produced for the NE-213 counter over the threshold region from 0.3 MeV ee to 0.8 MeV ee. The analyses produced yield spectra which were the same for thresholds of 0.6 and 0.8 MeV ee. Pulse-height analysis thresholds for the NE-102 counters were set at 3.0 MeV ee (= 6.8-MeV proton energy[7]) and at 0.6 MeV ee (= 2.0-MeV proton energy[2]) for the NE-213 counter for the yields reported here. These thresholds provide the lowest-energy neutron spectra possible while remaining consistent with the neutron yields of the higher-threshold analyses.

C. Energy resolutions

For measurements of neutron energies by the TOF method, the fractional energy resolution $\Delta T/T$ is given by the expression

$$\frac{\Delta T}{T}=\frac{(2M+T)(M+T)}{M^2}\left[\left(\frac{\Delta t}{t}\right)^2+\left(\frac{(1-\beta n)\Delta x}{x}\right)^2\right]^{1/2} \quad (1)$$

with

$$t=x/\beta c\ .$$

Here T is the neutron kinetic energy, M is the neutron rest mass, Δx is the uncertainty in the neutron flight path x arising from the finite dimensions of the counter, and n is the refractive index of the scintillator material. The effective thickness of the neutron counter is reduced from the physical thickness Δx by the factor $(1-\beta n)$. The finite thickness of the counter contributes to the energy resolution only because there exists a difference between the neutron speed and the speed of light in the scintillator. The time dispersion Δt was taken as the observed full width at half maximum (FWHM) of the prompt gamma peak in each neutron TOF spectrum. The observed width includes contributions from the beam telescope, the neutron counter, and the thickness of the target. The observed (FWHM) time dispersions were 0.8 ns for the 12.7-cm diam 10.2-cm thick detectors, 1.0 ns for the 12.7-cm diam 21.6-cm thick detectors, 1.2 ns for the 22.9-cm diam 20.3-cm thick detector, and 2.3 ns for the NE-213 counter. The poor resolution of the NE-213 counter was probably the result of the age of the NE-213 scintillation liquid. The resolutions calculated from Eq. (1) were used to determine the widths of the energy bins for the yield spectra reported in Sec. IV.

D. Conversion to energy spectra

The prompt gamma peak in each spectrum provided a reference point for calculating absolute neutron flight times. The background-subtracted TOF spectra were converted to energy spectra with bin widths equal to integral and fractional multiples of the experimental energy resolution. The smallest bin widths revealed no rapidly varying structure as a function of energy; consequently, the spectra are presented at integral multiples of the experimental energy resolutions to increase the statistics in each bin. The NE-213 detector was binned at the experimental energy resolution. For the NE-102 counters at neutron energies below 50 MeV, the energy bins are twice the energy resolutions; at neutron energies above 50 MeV, the multiple is two for the 30, 45, 60, and 90 deg spectra and three for the 0 and 6 deg spectra. To produce the absolute yields, each energy spectrum was divided by the number of alphas incident on the target, the calculated neutron detector efficiency, and the detector solid angle. The mean solid angle was calculated from the measured distance from the center of the target to the center of the neutron counter. The solid angles varied from about 0.5 msr for a 12.7-cm diam counter at 5 m to 2.0 msr for the 5.1-cm diam counter at 1 m.

E. Neutron detector efficiency calculations

The neutron detection efficiency of each counter was calculated with the Monte Carlo code of Cecil *et al.*[2] Calculations with this code provide good agreement with many experimental measurements of neutron detector efficiencies for neutron energies from about 1 to 300 MeV and for detector thresholds from about 0.1 to 22 MeV ee.[2] The calculated efficiencies used for the different neutron counters of this experiment are plotted in Fig. 3.

F. Corrections

The livetime was measured directly as the ratio of the actual number of events recorded by the computer data-acquisition system to the number of scaled neutron events detected by the neutron counters. The resultant deadtime correction was typically 1 to 3 percent.

The number of alphas incident on the target was measured as the number of beam-telescope coincidences. The incident beam rate was kept below 2×10^5 particles per second to keep the calculated correction for the occurrence of two or more beam ions per observed micropulse below

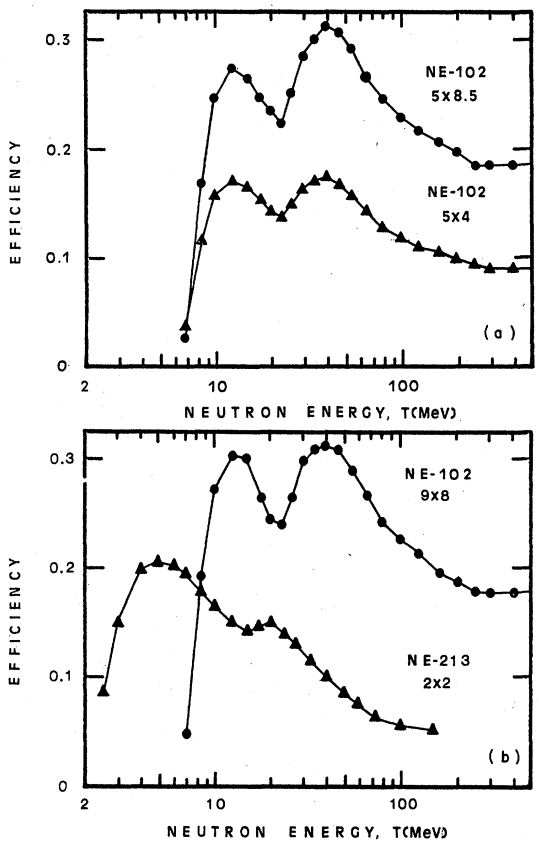

FIG. 3. Neutron detector efficiencies calculated with the Monte Carlo computer code[2]) for (a) a 12.7 cm diam by 21.6 cm thick NE-102 counter and a 12.7 cm diam by 10.2 cm thick NE-102 counter both with thresholds set at 3 MeV equivalent-electron energy, and (b) for a 22.9 cm diam by 20.9 cm thick NE-102 counter and a 5.1 cm diam by 5.1 cm thick NE-213 counter with thresholds set at 3 and 0.6 MeV equivalent-electron energies, respectively. The straight lines connecting the calculated points indicate interpolations used in the data analysis.

two percent. The correction C is

$$C=\sum_{n=2}^{\infty}\frac{(n-1)f_a(n)}{1-f_a(0)}, \tag{2}$$

where $f_a(n)$ is the Poisson probability for the observation of n particles in one micropulse with an average probability per micropulse of a. Note that the factor $(n-1)$ in Eq. (2) corrects for miscounting of alpha particles when the micropulse contains more than two alpha particles. The average probability a is given by the 78 ns period between micropulses divided by the mean time between alpha particles. The stochastic extractor in the cylcotron was adjusted to maximize the macroscopic duty cycle, which was greater than 50 percent. Since the probability of two or more alphas per micropulse was always less than 2%, the effect on the time resolution was ignored.

TABLE III. Scale uncertainties.

Source		Percent uncertainty	
Number of alphas		2	
Efficiency		5	
Background		7	
Target:	Steel/lead	Carbon	Water
Solid-angle [a]	1(3)	4(6)	6(9)
Total [a]	9(9)	10(11)	11(13)

[a] Numbers in parentheses are for the NE-213 counter.

G. Experimental uncertainties

The experimental uncertainties have been divided into two categories, those which scale an entire spectrum and those which are associated with a particular point or energy bin of the yield spectra and are primarily statistical. The statistical uncertainty is shown as a vertical error bar for each point of the reported yield spectra. The scale uncertainties are summarized in Table III. The uncertainty in the number of alphas incident on the target is composed entirely of the estimated error in the calculated beam pileup of particles in the beam telescope. The uncertainty in the Monte Carlo calculation of the efficiencies is estimated to be about 4 percent for a well-known threshold.[2] An uncertainty estimated to be about 3 percent in the pulse-height threshold results in an additional uncertainty in the efficiencies of about 3 percent at neutron energies near threshold. A net uncertainty of 5 percent in the efficiency results from the quadrature sum of these two quantities. As a percentage of the total yield, the background decreases typically from about 25 percent at a low energy (at twice threshold) to only about 2 percent at high energies. Since we estimate that the uncertainty in the background is about 25 percent, this uncertainty produces an uncertainty in the extracted yield that is typically less than 7 percent. The uncertainty in the solid angle is dominated by the uncertainty in the position of production of a neutron in the thick targets. An upper bound on the uncertainty in the solid angle is equal to the difference in solid angle for a point at the extremity of the target and the solid angle for a point at the center of the target. One-half of this calculated upper bound on the uncertainty in the solid angle is taken as the estimated uncertainty in the solid angle. The resulting uncertainties in the solid angle for the steel/lead, carbon, and water targets are 1, 4, and 6 percent, respectively, for the high-energy (NE-102) measurements and 3, 6, and 9 percent, respectively, for the low-energy (NE-213) measurements.

IV. YEILD SPECTRA

The yield spectra are presented in Tables IV through VII. The differential neutron yields from 710-MeV alphas measured with the NE-102 counters are presented in Table IV starting at about 10 MeV and extending to the highest neutron energies observed. Differential neutron yields from 710-MeV alphas measured with the NE-213 counter are presented in Tables V and VI starting at about 3 MeV and extending to about 50 MeV. The measured neutron yields from 640-MeV alphas are presented in Table VII. The statistical uncertainties in the data points are indicated following each datum. The energy corresponding to each point is the mean energy of an energy bin whose width extends halfway to the nearest neighboring data points.

The yields reported here include neutrons produced in the target by the interactions of primary neutrons and secondary charged particles. The effects of neutron scattering in the target are included also. An accurate separation of these effects to reveal the primary neutron spectra would require a Monte Carlo simulation of the neutron and charged particle transport through the target. The consequences of these finite-target size effects are estimated to be large only at low energies and are not separated in the yields reported here.

Some of the neutron spectra produced by 710-MeV incident alphas are plotted in Figs. 4 through 8. These spectra are distinctly forward peaked with the lighter (carbon and water) targets (Figs. 4 and 5) having a somewhat larger proportion of their yield in the forward direction than the heavier (steel and lead) targets (Figs. 6, 7, and 8). For angles less than 30 deg, there is a significant yield of neutrons with energies greater than the 177 MeV per nucleon of the incident alphas. The 0-deg spectra from carbon and water have a large bump in their neutron yield spectra at about 120 MeV. The 0-deg spectra from the steel and lead targets show a somewhat smaller bump in the neutron yield at about the same energy. The 6, 15, and 30-deg spectra for all the targets show progressively smaller bumps at somewhat lower neutron energies. For angles larger than 30 deg, the yield spectra decrease uniformly with increasing neutron energy and angle. Neutron yields for energies down to about 3 MeV, measured with the single NE-213 counter, are shown at 45 deg for carbon, water, and steel targets and at 0, 45, and 90 deg for the lead target. Because the targets were placed at an angle to the incoming alpha beam, the neutron attenuation was, in general, different for the NE-213 and NE-102 detector measurements performed at the same

TABLE IV. Neutron yields from 710-MeV alphas stopping in carbon, water, steel, and lead targets.

Energy (MeV)	Neutron yield (Neuts/10^6 alphas MeV sr) [a] Carbon		Water		Steel		Lead	
				0 deg				
10.0	2250	(8.5)	2430	(10.0)	2470	(16.0)	3850	(5.4)
12.3	2380	(6.5)	2150	(8.6)	2430	(13.0)	3340	(4.9)
15.0	2480	(5.5)	1960	(7.9)	2570	(11.0)	2940	(4.6)
18.5	2210	(5.3)	1860	(7.2)	2250	(10.0)	2640	(4.4)
22.8	2780	(4.1)	2280	(5.6)	1840	(10.0)	2590	(4.0)
28.2	2740	(3.4)	2360	(4.4)	1760	(8.2)	2030	(3.7)
35.2	2850	(2.8)	2560	(3.6)	2050	(6.3)	2030	(3.2)
44.3	3180	(2.3)	2930	(2.8)	2070	(5.3)	1920	(2.8)
56.5	3920	(1.8)	3730	(2.2)	2380	(4.3)	1900	(2.5)
68.6	4720	(2.0)	4780	(2.4)	2740	(5.0)	2070	(2.9)
79.8	5740	(1.7)	5640	(2.1)	3150	(4.3)	2290	(2.6)
93.7	6340	(1.5)	6500	(1.8)	3600	(3.7)	2430	(2.3)
111.0	7190	(1.3)	7110	(1.6)	4130	(3.2)	2590	(2.0)
134.0	6900	(1.2)	6640	(1.4)	3850	(2.9)	2370	(1.9)
165.0	5260	(1.2)	4470	(1.5)	3000	(2.9)	1890	(1.8)
207.0	2370	(1.5)	1930	(2.0)	1350	(3.6)	865	(2.3)
268.0	488	(2.7)	369	(3.8)	242	(7.2)	170	(4.4)
363.0	40.2	(7.9)	29.5	(12.0)	15.3	(27.0)	14.7	(13.0)
525.0	2.4	(32.0)						
				6 deg				
10.0	2610	(7.9)			3390	(11.0)	4850	(5.0)
12.3	2450	(6.6)			2770	(11.0)	3450	(5.0)
15.0	2470	(5.6)			2220	(11.0)	3210	(4.5)
18.5	2510	(5.0)			2480	(8.9)	3030	(4.1)
22.8	2890	(4.1)			2700	(7.6)	2660	(4.0)
28.2	2620	(3.5)			1930	(7.4)	2250	(3.5)
35.2	2790	(2.9)			1870	(6.4)	2040	(3.2)
44.3	2940	(2.4)			2100	(5.1)	1930	(2.7)
56.5	3300	(2.0)			2280	(4.3)	1910	(2.4)
68.6	3820	(2.3)			2270	(5.4)	2020	(2.9)
79.8	4300	(2.0)			2630	(4.7)	2020	(2.7)
93.7	4450	(1.8)			2480	(4.5)	2110	(2.5)
111.0	4470	(1.7)			2470	(3.9)	2080	(2.3)
134.0	4190	(1.5)			2540	(3.6)	1780	(2.2)
165.0	3080	(1.6)			1820	(3.7)	1350	(2.2)
207.0	1550	(1.9)			902	(4.5)	637	(2.7)
268.0	406	(3.0)			244	(7.1)	165	(4.4)
363.0	50.0	(7.0)			30.7	(17.0)	18	(12.0)
525.0	2.5	(29.0)						
				15 deg				
11.4	2540	(4.9)	1720	(7.4)	2640	(8.7)	4240	(3.5)
14.6	2550	(3.9)	1890	(5.6)	2610	(7.4)	3250	(3.4)
18.6	2510	(3.5)	2140	(4.5)	2210	(7.0)	2520	(3.5)
23.6	2680	(3.0)	2070	(4.1)	2100	(6.4)	2460	(3.1)
29.9	2480	(2.5)	1980	(3.3)	1980	(5.2)	2010	(2.8)
37.8	2450	(2.2)	1980	(2.8)	1870	(4.6)	1820	(2.5)
47.6	2430	(1.9)	1990	(2.5)	1790	(4.1)	1690	(2.2)
56.7	2590	(2.3)	2050	(3.1)	1780	(5.2)	1640	(2.8)
64.3	2650	(2.2)	2190	(2.8)	1940	(4.7)	1560	(2.7)
72.9	2660	(2.1)	2170	(2.8)	1770	(4.8)	1500	(2.7)
83.0	2480	(2.1)	2030	(2.7)	1660	(4.7)	1360	(2.7)
94.9	2300	(2.0)	1870	(2.6)	1530	(4.5)	1290	(2.6)
109.0	1960	(2.0)	1650	(2.6)	1330	(4.5)	1010	(2.7)
126.0	1580	(2.1)	1340	(2.6)	988	(4.8)	851	(2.7)
147.0	1050	(2.3)	925	(2.9)	732	(5.1)	558	(3.0)

TABLE IV. *(Continued.)*

Energy (MeV)	Neutron yield (Neuts/10^6 alphas MeV sr) [a] Carbon	Water	Steel	Lead
		15 deg		
172.0	578 (2.9)	518 (3.5)	378 (6.5)	317 (3.7)
205.0	271 (3.7)	236 (4.6)	146 (9.3)	133 (5.2)
249.0	91.9 (5.6)	78.3 (7.2)	50.6(14.0)	46.4 (8.1)
309.0	16.3(12.0)	14.3(16.0)		5.1(30.0)
		30 deg		
11.4	2180 (5.5)	1850 (7.5)	3020 (8.2)	4330 (3.6)
14.6	2260 (4.3)	1560 (6.7)	2410 (7.7)	2840 (3.9)
18.6	2100 (4.0)	1550 (5.8)	2260 (7.1)	2320 (3.9)
23.6	2130 (3.5)	1690 (4.8)	1670 (7.5)	2150 (3.5)
29.9	1790 (3.0)	1370 (4.2)	1510 (6.2)	1790 (3.0)
37.8	1590 (2.7)	1380 (3.5)	1230 (5.9)	1360 (3.0)
47.6	1520 (2.4)	1230 (3.3)	1290 (4.9)	1220 (2.7)
56.7	1440 (3.2)	1250 (4.0)	1050 (6.9)	1040 (3.7)
64.3	1480 (3.0)	1210 (3.9)	985 (6.8)	1000 (3.5)
72.9	1340 (3.0)	1270 (3.7)	891 (6.9)	938 (3.5)
83.0	1180 (3.0)	1120 (3.7)	710 (7.3)	767 (3.6)
94.9	911 (3.3)	832 (4.0)	615 (7.3)	635 (3.7)
109.0	620 (3.7)	589 (4.5)	421 (8.3)	413 (4.4)
126.0	425 (4.1)	386 (5.1)	279 (9.5)	272 (5.0)
147.0	272 (4.7)	236 (6.0)	184 (11.0)	143 (6.6)
172.0	133 (6.2)	126 (7.6)	104 (13.0)	87.1 (7.8)
205.0	55.3 (8.8)	50.1(11.0)	38.2(21.0)	33.8(12.0)
249.0	19.2(14.0)	14.8(21.0)		
		45 deg		
11.1	1650 (3.3)	1370 (4.7)	2260 (5.1)	3270 (2.3)
14.1	1410 (3.0)	1290 (3.9)	1590 (5.2)	2320 (2.4)
17.9	1380 (2.7)	1250 (3.5)	1410 (5.0)	1720 (2.6)
22.7	1270 (2.5)	1200 (3.1)	1280 (4.7)	1530 (2.4)
28.6	1080 (2.2)	1020 (2.7)	1000 (4.3)	1210 (2.2)
36.2	893 (2.1)	875 (2.5)	842 (4.0)	944 (2.1)
45.9	791 (1.9)	780 (2.3)	696 (3.8)	712 (2.1)
54.9	683 (2.6)	682 (3.0)	549 (5.4)	568 (2.9)
62.7	582 (2.7)	588 (3.1)	573 (5.0)	516 (2.9)
71.8	510 (2.7)	485 (3.2)	460 (5.3)	411 (3.0)
82.8	426 (2.7)	401 (3.3)	326 (6.0)	335 (3.2)
96.2	327 (2.9)	299 (3.6)	275 (6.0)	255 (3.4)
113.0	219 (3.3)	210 (4.0)	162 (7.4)	154 (4.1)
133.0	131 (3.9)	126 (4.7)	99.5 (8.7)	88.9 (5.1)
159.0	59.8 (5.3)	52.4 (6.8)	40.9(13.0)	36.1 (8.0)
194.0	22.3 (7.9)	21.0(10.0)	17.3(19.0)	12.5(14.0)
239.0	6.1(15.0)	5.6(20.0)		
		60 deg		
10.5	908 (8.2)	819 (8.9)	1360 (6.5)	1930 (4.9)
13.0	765 (7.4)	799 (7.2)	1230 (5.6)	1300 (5.1)
16.2	777 (6.5)	702 (6.8)	888 (6.1)	999 (5.3)
20.3	699 (6.2)	690 (6.2)	797 (5.9)	789 (5.5)
25.5	584 (5.9)	617 (5.6)	605 (6.0)	590 (5.6)
32.3	540 (5.0)	560 (4.8)	516 (5.2)	463 (5.0)
41.3	402 (4.7)	421 (4.5)	375 (5.0)	346 (4.7)
53.5	319 (4.7)	311 (4.6)	298 (5.0)	255 (4.8)
65.8	251 (6.5)	213 (6.9)	226 (7.0)	168 (7.6)
77.2	220 (6.6)	174 (7.3)	177 (7.5)	130 (8.3)
91.7	146 (7.3)	107 (8.5)	112 (8.6)	80.8(10.0)
110.0	68.7(10.0)	74.4 (9.4)	59.8(11.0)	58.6(11.0)
135.0	37.4(12.0)	34.9(13.0)	28.8(14.0)	15.9(25.0)

TABLE IV. *(Continued.)*

Energy (MeV)	Neutron yield (Neuts/10^6 alphas MeV sr) [a] Carbon	Water	Steel	Lead
		60 deg		
169.0	19.2(15.0)	13.1(19.0)	11.8(21.0)	
217.0	4.2(31.0)			
		90 deg		
13.2	574 (3.9)	550 (3.7)	964 (3.8)	1160 (2.2)
17.8	417 (4.0)	366 (4.1)	579 (4.5)	640 (2.7)
23.8	377 (3.7)	307 (3.9)	496 (4.4)	458 (2.8)
31.8	250 (3.5)	168 (4.2)	319 (4.3)	262 (2.9)
42.3	143 (3.8)	110 (4.3)	173 (4.9)	155 (3.2)
56.2	86.6 (4.4)	56.9 (5.4)	111 (5.6)	87.4 (3.9)
69.4	47.0 (7.7)	34.7 (9.0)	56.8(10.0)	49.1 (7.1)
81.6	25.6 (9.8)	20.5(11.0)	39.8(12.0)	30.6 (8.7)
96.7	12.9(14.0)	13.5(13.0)	29.9(13.0)	17.0(12.0)
115.0	6.9(18.0)	6.0(20.0)	11.9(21.0)	9.4(17.0)
139.0			4.7(33.0)	
		120 deg		
13.2	393 (4.7)	330 (4.8)	792 (3.0)	1190 (2.1)
17.8	283 (4.9)	234 (5.0)	420 (3.7)	622 (2.7)
23.8	182 (5.5)	150 (5.5)	290 (4.0)	330 (3.4)
31.8	91.1 (6.1)	68.8 (6.5)	148 (4.4)	173 (3.7)
42.3	39.6 (8.0)	32.7 (8.1)	72.8 (5.3)	74.6 (5.1)
56.2	15.3(12.0)	11.6(13.0)	28.2 (7.9)	33.5 (7.6)
69.4	11.0(18.0)	6.0(25.0)	12.9(16.0)	13.1(19.0)
81.6			6.9(21.0)	10.2(20.0)
		150 deg		
12.8	347 (2.7)	222 (3.3)	648 (1.9)	1080 (1.2)
17.1	218 (3.0)	148 (3.5)	348 (2.3)	483 (1.8)
22.8	133 (3.5)	81.3 (4.4)	192 (2.9)	255 (2.3)
30.4	55.7 (4.4)	38.5 (5.2)	83.8 (3.6)	108 (3.1)
40.7	21.7 (6.1)	15.0 (7.4)	31.8 (5.1)	40.9 (4.7)
54.7	7.5(10.0)	6.0(11.0)	9.4 (9.6)	12.0(10.0)
68.7				4.0(30.0)

[a] Percent uncertainties (in parentheses) are statistical only. The yields include neutrons produced by the interactions of primary neutrons and secondary charged particles as well as the effects of neutron scattering in the thick targets (see text).

angles, but on the opposite sides of the beam line. For purposes of comparison the NE-213 spectra were adjusted to have the same neutron attenuation in the target as the corresponding NE-102 spectra. This adjustment was approximated using the inelastic neutron cross sections for each target.[8,9] The reported yields increase at the lower energies for all of the targets but most rapidly for the lead target; in addition, the angular distribution of low-energy neutrons becomes almost isotropic for the lead target.

The basic characteristics of the spectra are consistent with the simple idea that the high-energy neutrons are produced primarily by direct-reaction processes and the low-energy neutrons by evaporation processes. For the light targets, the direct-reaction products are more likely to escape the nucleus without being absorbed to form compound nuclei. Thus, the carbon and water spectra at the most forward angles show pronounced peaks somewhat below the kinetic energy per nucleon. For the heavier targets of steel and lead, this high-energy peak is suppressed.

Neutron spectra measured at angles of 0, 45, 90, and 150 deg from 640-MeV alphas stopping in a lead target are presented in Fig. 9. These spectra are similar to the 710-MeV spectra except that they are reduced in magnitude. The spectra are forward peaked and there is a bump in the zero-degree spectrum at about 120 MeV. The yields for angles of 90 deg and larger decrease uniformly with increasing neutron energy.

TABLE V. Neutron yields at low energies from 710-MeV alphas stopping in a lead target. [a]

Energy (MeV)	Neutron yield (Neuts/10^6 alphas MeV sr) 0 deg	90 deg	135 deg	
3.39	31 600(2.6)	17 800(3.2)	19 000	(2.7)
3.91	23 500(2.6)	13 400(3.2)	15 100	(2.6)
4.52	17 600(2.7)	9 100(3.4)	11 300	(2.7)
5.27	13 500(3.8)	6 670(3.6)	8 120	(2.8)
6.18	10 200(3.0)	4 880(3.9)	5 780	(3.1)
7.32	7 900(3.1)	3 590(4.1)	4 030	(3.4)
8.79	5 750(3.7)	2 490(4.6)	2 920	(3.7)
10.6	4 230(3.8)	1 670(5.2)	1 870	(4.3)
13.1	3 470(3.8)	1 180(5.8)	1 210	(5.1)
16.3	2 510(3.8)	772(6.1)	709	(5.7)
20.9	2 080(3.3)	491(6.4)	399	(6.4)
27.3	1 700(3.2)	298(7.2)	208	(8.0)
37.1	1 690(2.7)	230(7.2)	136	(8.8)
52.9	1 690(2.3)	141(8.2)	80.1	(10.0)

[a] See Table VI for yields at 45 deg. Percent uncertainties (in parentheses) are statistical only. The yields include neutrons produced by the interactions of primary neutrons and secondary charged particles as well as the effects of neutron scattering in the thick targets (see text).

V. COMPARISON WITH INTRANUCLEAR-CASCADE-MODEL CALCULATIONS

The neutron spectra from alpha bombardment of a stopping oxygen target were calculated using an intranuclear-cascade and evaporation model[1] of the nucleon interactions. The calculation was performed as a series of thin-target calculations which were then summed to obtain the neutron yields from alphas stopping in the thick target. The neutron yields from a water target are shown compared with these calculations in Fig. 5. The calculations are for a range of angles centered about the angle of the experimental measurement. There is good agreement between the calculations and the measured spectra at the forward angles. The 0- to 10-deg calculation falls midway between the measured 0- and 15-deg spectra. The agreement of the 30- to 60-deg calculation with the 45-deg measurement is excellent. The spectra measured at 90 and 120 deg have different shapes from the calculated spectra. The 90-deg calculations are significantly less than the measured yields.

The prominent bumps seen in the neutron spectra at forward angles near 120 MeV are apparently the result of peripheral reactions (with large impact parameters) between the projectile and target nuclei. These reactions often result in quasi-free elastic scattering of the target and projectile nucleons. The intranuclear-cascade calculations for a thin target show quasi-free elastic scattering peaks at the incident beam energy per nucleon minus the nuclear binding energy of a neutron. For a stopping target, the production contributions of several thin targets are added together at increasingly lower energies. The resultant quasi-free bump appears at about 120 MeV, in good agreement with the measured spectra.

The high-energy tails of the small-angle neutron spectra extend to nearly twice the energy per nucleon of the incident alphas. The magnitude of the high-energy tails of the 0- and 6-deg spectra are nearly the same. These characteristics of the measured spectra at high energies are consis-

TABLE VI. Low-energy neutron yields at 45° from 710-MeV alphas stopping in carbon, water, steel, and lead targets.

Energy (MeV)	Neutron yield (Neuts/10^6 alphas MeV sr) [a] Carbon	Water	Steel	Lead
3.39	3040(7.0)	2420(7.9)	10 100(4.6)	35 900(2.2)
3.91	2960(6.0)	2320(6.7)	7 200(4.7)	26 900(2.2)
4.52	3120(5.0)	2050(6.3)	5 930(4.6)	21 100(2.2)
5.27	2370(5.2)	1880(5.8)	4 600(4.7)	15 500(2.4)
6.18	2040(5.2)	1630(5.8)	4 040(4.5)	11 700(2.5)
7.32	1810(5.0)	1400(5.6)	3 000(4.8)	8 510(2.7)
8.79	1440(5.2)	1180(5.6)	2 490(4.9)	5 900(3.0)
10.60	1410(4.8)	1230(5.0)	2 060(5.0)	4 670(3.1)
13.10	1440(4.4)	1400(4.3)	1 620(5.2)	3 350(3.4)
16.30	1220(4.0)	1160(4.0)	1 230(5.0)	2 400(3.4)
20.90	974(3.7)	959(3.6)	1 000(4.5)	1 620(3.4)
27.30	866(3.4)	858(3.3)	760(4.5)	1 240(3.4)
37.10	760(3.2)	792(3.0)	694(4.0)	1 090(3.2)
52.90	681(3.0)	658(3.0)	601(3.8)	802(3.3)

[a] Percent uncertainties (in parentheses) are statistical only. The yields include neutrons produced by the interactions of primary neutrons and secondary charged particles as well as the effects of neutron scattering in the thick targets (see text).

TABLE VII. Neutron yields from 640-MeV alphas stopping in a lead target.

Energy (MeV)	Neutron yield [a] (Neuts/10^6 alphas MeV sr)	Energy (MeV)	Neutron yield [a] (Neuts/10^6 alphas MeV sr)
	0 deg		45 deg
10.0	3 630 (9.4)	27.30	655 (5.5)
12.3	3 500 (8.0)	37.10	505 (5.5)
15.0	2 390 (8.8)	52.90	390 (5.6)
18.5	1 910 (9.1)		
22.8	1 900 (8.3)		90 deg
28.2	1 900 (6.7)	13.2	581 (5.2)
35.2	1 520 (6.4)	17.8	381 (5.7)
44.3	1 540 (5.4)	23.8	257 (6.2)
56.5	1 530 (4.8)	31.8	141 (6.5)
68.6	1 530 (6.0)	42.3	94.4 (6.6)
79.8	1 810 (5.1)	56.2	46.7 (8.5)
93.7	1 830 (4.7)	69.4	29.5(14.0)
111.0	1 770 (4.3)	81.6	19.0(16.0)
134.0	1 620 (4.0)		
165.0	1 040 (4.4)		120 deg
207.0	332 (6.7)	13.2	953 (3.9)
268.0	62.1(13.0)	17.8	560 (4.5)
		23.8	273 (6.0)
	45 deg	31.8	141 (6.5)
3.39	18 600 (3.7)	42.3	51.7 (9.5)
3.91	12 800 (3.8)	56.2	21.7(14.0)
4.52	10 000 (3.8)	69.4	10.3(28.0)
5.27	7 270 (4.1)		
6.18	5 260 (4.4)		150 deg
7.32	4 210 (4.4)	12.8	905 (2.2)
8.79	2 880 (5.0)	17.1	416 (3.0)
10.60	2 180 (5.3)	22.8	200 (4.2)
13.10	1 620 (5.7)	30.4	87.5 (5.1)
16.30	1 080 (6.0)	40.7	24.6 (9.2)
20.90	857 (5.5)	54.7	8.2(17.0)

[a] Percent uncertainties (in parentheses) are statistical only. The yields include neutrons produced by the interactions of primary neutrons and secondary charged particles as well as the effects of neutron scattering in the thick targets (see text).

tent with the production mechanism proposed by Bertini[10] in which a free nucleon from the dissociated incident ion interacts with the tangential component of the fermi momentum of a nucleon in the target.

Calculations based on classical equations of motion[11] suggest that central collisions (with small impact parameters) of heavy ions with nuclei result in an isotropic distribution in the center-of-mass system of the emitted particles. Much of the initial kinetic energy of the heavy ion is dissipated in the prolific production of particles. This effect is observed in the measured neutron spectra which become more nearly isotropic at low energies.

In Table VIII, we list the total integrated neutron yield above 10 MeV for each of the targets. There are about 0.5 neutrons above 10 MeV per incident alpha, relatively independent of the target nucleus. The flux in the backward hemisphere increases as the atomic number of the target increases and is only 10 to 20 percent of the total flux. The NE-213 measurements on lead at angles of 0, 45, 90, and 135 deg were used in conjunction with the NE-102 measurements to obtain the angle-integrated neutron yields above 3.0, 5.0, 10.0, 20.0, and 50.0 MeV. These data are shown in Fig. 10 and are well represented by the simple

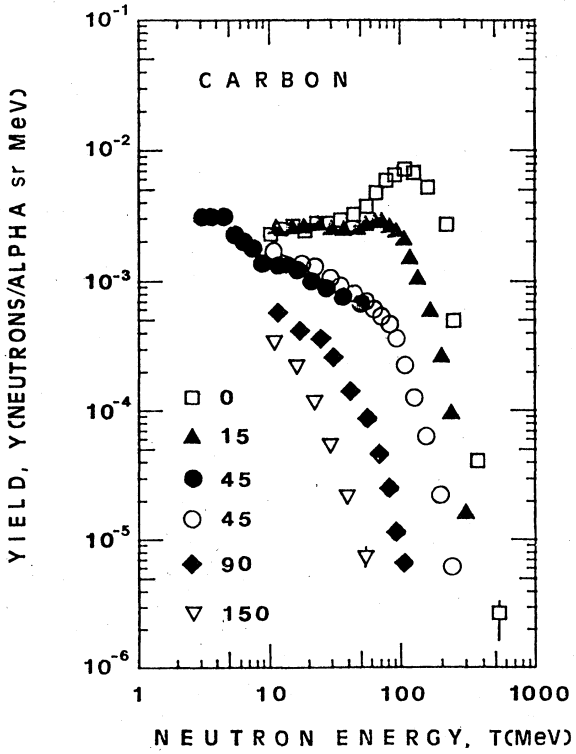

FIG. 4. Neutron yield spectra at laboratory angles of 0, 15, 45, 90, and 150 deg from 710-MeV alphas stopping in a carbon target. The data shown as solid circles are from the NE-213 detector.

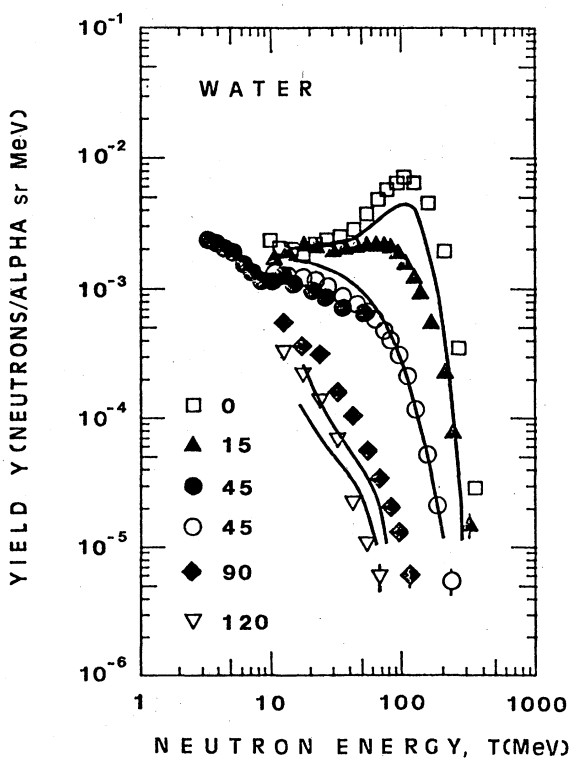

FIG. 5. Neutron yield spectra at laboratory angles of 0, 15, 45, 90, and 120 deg from 710-MeV alphas stopping in a water target compared with Monte Carlo intranuclear-cascade calculations for alphas interacting in an oxygen target. The four calculations shown as the solid lines are averaged over the angular ranges 0–10, 30–60, 80–110, and 110–130 deg, respectively. The data represented by solid circles are from the NE-213 counter.

power law

$$Y[>T\ (\mathrm{MeV})] = 2.35T^{-0.65}. \quad (3)$$

The total yield of neutrons above 3.0 MeV for the lead target is about 1.2 neutrons per incident alpha.

VI. SUMMARY

We measured neutron angular and energy distributions produced by 710-MeV alphas stopping in targets of water, carbon, steel, and lead, and 640-MeV alphas stopping in a lead target. Measurements are presented for neutron energies as low as 3 MeV and up to about 300 MeV. The neutron angular distributions are forward peaked with a broad bump at about 120 MeV in the 0- and 6-deg spectra. Also the 0- and 6-deg neutron spectra have significant yields of neutrons above the kinetic energy per nucleon of the incident alpha beam. The 640-MeV spectra are similar to the 710-MeV spectra but the 640-MeV yields are reduced in magnitude by about 20 percent. The largest source of uncertainty in these measurements is associated with the contribution of room-scattered neutrons to the subtracted backgrounds. The overall uncertainty in the absolute normalization of these data is estimated to vary from about 9 to 13 percent. The statistical uncertainty of the data is typically 5 percent.

These measurements are important for the design of beam dumps and shielding for medium-energy heavy-ion accelerators. The neutron spectra from alphas stopping in carbon and water targets are of interest also for estimating neutron background doses in heavy-ion cancer radiotherapy. The calculations of an intranuclear-cascade model for an oxygen target are consistent with the measurements for the water target at forward angles but are always smaller than the measured yields at backward angles.

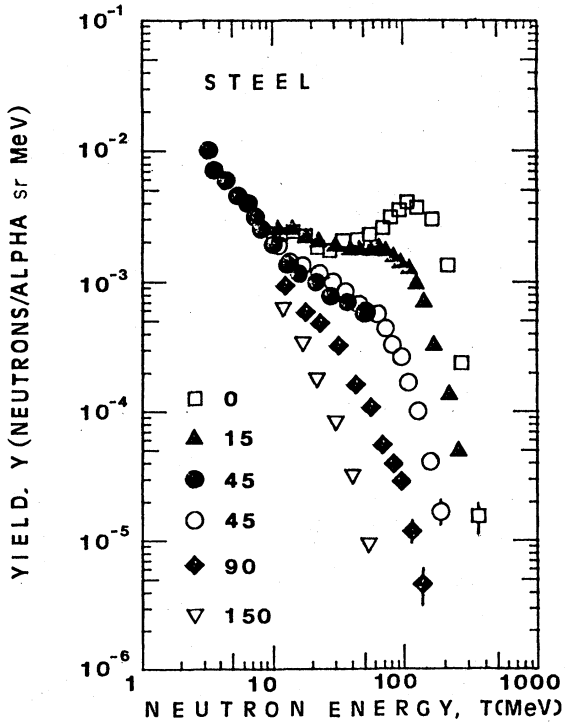

FIG. 6. Neutron yield spectra at laboratory angles of 0, 15, 45, 90, and 150 deg from 710-MeV alphas stopping in a steel target. The data shown as solid circles are from the NE-213 counter.

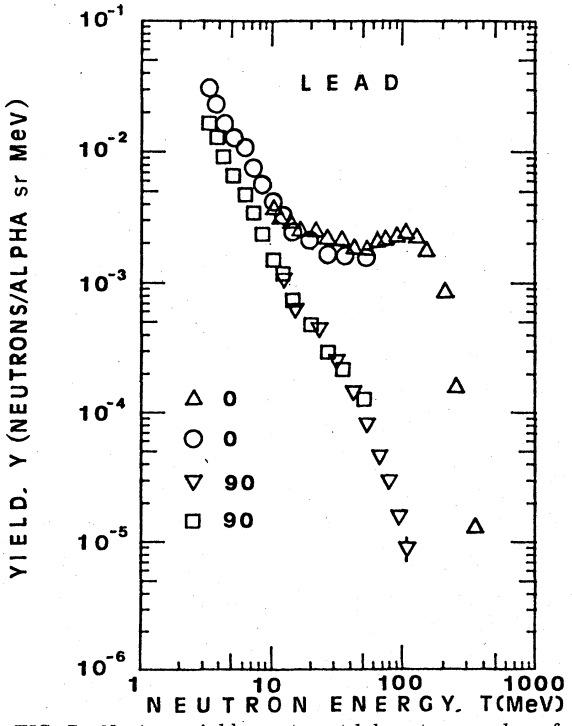

FIG. 7. Neutron yield spectra at laboratory angles of 0 and 90 deg from 710-MeV alphas stopping in a lead target. The data shown as squares and circles are from the NE-213 counter.

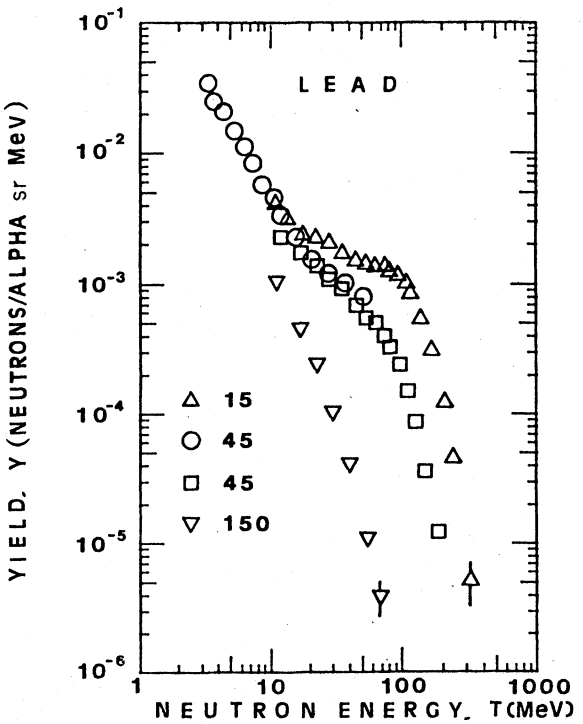

FIG. 8. Neutron yield spectra at laboratory angles of 15, 45, and 150 deg from 710-MeV alphas stopping in a lead target. The data shown as circles are from the NE-213 counter.

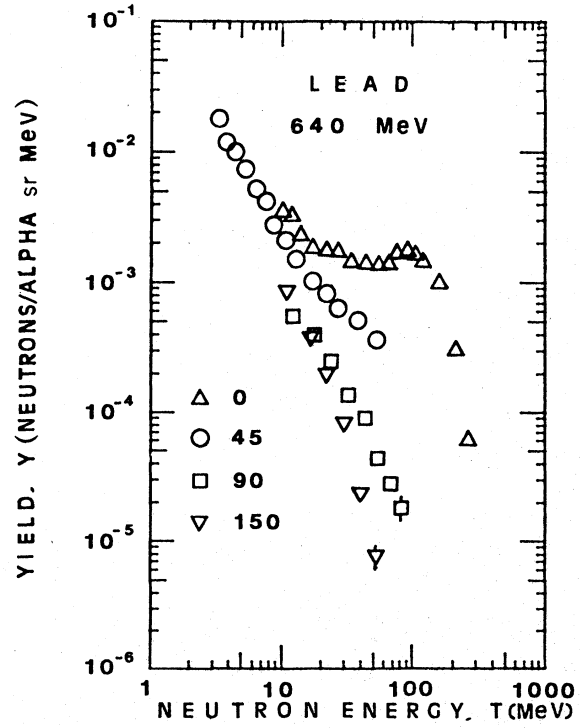

FIG. 9. Neutron yield spectra at laboratory angles of 0, 45, 90, and 150 deg from 640-MeV alphas stopping in a lead target. The data shown as circles are from the NE-213 counter.

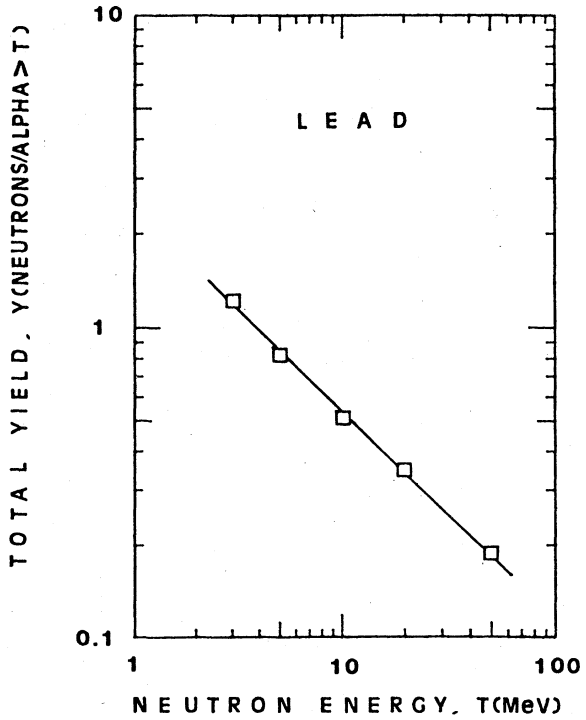

FIG. 10. The angle-integrated neutron yields above a given energy from 710-MeV alphas stopping in a lead target.

TABLE VIII. Neutrons above 10 MeV per 100 alphas.

Target	Total	Forward ($0 < \theta < 90$)	Backward ($90 < \theta < 180$)
Water	52	48	4
Carbon	58	54	4
Steel	51	44	7
Lead	51	43	8

ACKNOWLEDGMENTS

We gratefully acknowledge the support and advice of Professor N. S. Wall of the University of Maryland during the preliminary stage of this experiment and the support and assistance of the staff at the Space Radiation Effects Laboratory during the running of this experiment. We thank Dr. T. A. Gabriel of Oak Ridge National Laboratory for performing heavy-ion cascade calculations for us. This work was supported in part by the Department of Energy under Contract No. EY-76-S-02-2231 and the National Science Foundation under Grants Nos. PHY-75-02870, PHY-79-07790, PHY-76-02206, and PHY-78-01684.

*Present address: Jet Propulsion Laboratory, 4800 Oak Grove Drive, Pasadena, California 91103.

†Present address: Department of Radiation Therapy and Nuclear Medicine, Thomas Jefferson University, Philadelphia, Pennsylvania 19107.

[1]T. A. Gabriel, private communication, calculations done with the code HIC-1, described in H. W. Bertini, T. A. Gabriel, R. T. Santoro, D. W. Herman, N. M. Larson, and J. M. Hunt, ORNL/TM-4134 (1974); H. W. Bertini, T. A. Gabriel, and R. T. Santoro, Phys. Rev. C 9, 522 (1974).

[2]R. A. Cecil, B. D. Anderson, R. Madey, Nucl. Instrum. Methods 161, 439 (1979).

[3]R. Madey and F. M. Waterman, Nucl. Instrum. Methods 106, 89 (1973).

[4]A. R. Baldwin and R. Madey, Nucl. Instrum. Methods 128, 557 (1975).

[5]R. Hartmann, H. P. Isaak, R. Engfer, E. H. Hermes, H. S. Pruys, W. Dey, H. J. Pfeiffer, U. Sennhauser, H. K. Walter, and J. Morgenstern, Nucl. Phys. A308, 345 (1978).

[6]H. Knox and T. Miller, Nucl. Instrum. Methods 101, 519 (1972).

[7]R. Madey, F. M. Waterman, A. R. Baldwin, J. D. Carlson, and J. Rapaport, Nucl. Instrum. Methods 151, 445 (1978).

[8]BNL 325, 3rd ed., Vol. 2, Brookhaven National Laboratories, Upton, New York, 1976.

[9]H. W. Patterson and R. H. Thomas, *Accelerator Health Physics* (Academic, New York, 1973).

[10]H. W. Bertini, R. T. Sanforo, and O. W. Hermann, Phys. Rev. C 14, 590 (1977).

[11]A. R. Bodmer and C. N. Panos, Phys. Rev. C 15, 1342 (1977).